Desalination and Water Treatment
www.deswater.com
doi: 10.5004/dwt.2022.28599

266 (2022) 173–185
August

Experimental design and optimization of textile dye photodiscoloration using Zn/TiO_2 catalysts

Luiz Eduardo Nochi Castro[a,*], Antonio Henrique Meira[a], Lariana Negrão Beraldo Almeida[b], Giane Gonçalves Lenzi[b], Leda Maria Saragiotto Colpini[a]

[a]*Federal University of Parana, Campus Avançado de Jandaia do Sul. Dr. João Maximiano, 426 Jandaia do Sul, PR, Brazil, Tel. +55 43 99675-0525; Fax: +55 43 3432-4551; emails: luiz_nc@yahoo.com (L.E.N. Castro), antoniorick1997@gmail.com (A.H. Meira), ledasaracol@ufpr.br (L.M.S. Colpini)*
[b]*Federal Technological University of Parana, Av. Monteiro Lobato, s/n – km 04, 84016-210, Ponta Grossa, PR, Brazil, emails: beraldolariana@gmail.com (L.N.B. Almeida), gianeg@utfpr.edu.br (G.G. Lenzi)*

Received 9 February 2022; Accepted 4 June 2022

ABSTRACT

The application potential of Zn/TiO_2 catalysts generated by the impregnation method in the photodiscoloration of the textile dye Orange 122 is investigated in this paper. The synthesis of the catalysts followed a 2^2 factorial design with repetition at the central point. N_2 adsorption measurements Brunauer–Emmett–Teller (BET method), scanning electron microscopy with energy dispersive X-ray, X-ray diffraction, and point of zero charge were the characterization techniques employed. The photocatalytic tests were carried out in batches in the presence of sunlight with dye solutions of 10 mg L^{-1}, kinetic data modeling, and statistical analysis for the data obtained in the solar assays, and catalyst reuse tests were carried out under artificial light under the same conditions as the sunlight test. The photocatalytic studies revealed that the calcination temperature of 200°C produced the greatest discoloration results for the Reactive Orange 122 dye (99.9%). The Behnajady–Modirshahla–Ghanbery model provided the greatest match for the discoloration kinetics, and statistical analysis revealed that the calcination temperature was the variable that influenced the discoloration assay results. The 6% Zn/TiO_2 catalyst showed approximately 33% discoloration after its fourth use, according to the results of the reuse tests.

Keywords: Impregnation; Photocatalysis; Reuse; Advanced oxidative process; Characterization; Orange 122

1. Introduction

Textile industries are now one of the most significant sources of water pollution; their effluents have a high organic load, particularly due to dyes, which are derived from the pretreatment of fabrics through dyeing and the posttreatment of fibers, resulting in a large amount of water and dyes being used and subsequently discarded as wastewater [1,2]. Dyes, in particular, have a strong coloring power, and when discarded, they color water bodies [3–5]. As a result, sunlight has a harder time reaching the water, causing damage to the respiration of fauna and flora and perhaps causing eutrophication of that environment [6,7].

Due to a lack of environmental management in the factories and the low effectiveness of dye fixation in the fibers, which is between 60%–90% [8,9], approximately 30% of all dye production in the world is produced in excess, with 10%–25% of those wasted in the dying process. Furthermore, according to some research, approximately 20% of the dye effluents produced by the textile industry are released into the environment without being treated [6,10]. The Reactive Orange 122 dye is one of the typical azo dyes

* Corresponding author.

found in textile industry effluents; this type of wastewater is highly recalcitrant, making degradation more difficult, especially due to the presence of chromophore groups in the chemical structure of this dye, one of which is the azo groups (–N=N–); this class of dyes is known as azo dyes, and it accounts for approximately 50%–70% of all dyes used in the textile industry [2,8,11].

Because some dyes and dye degradation products have been documented to be carcinogenic, toxic, nonbiodegradable, and mutagenic, especially when azo groups and phenolic groups are present, the effluent must be treated before being discharged into receiving environments [2,8,12,13]. Traditional biological treatments are inefficient due to the nature of these effluents, both in terms of coloring and effluent deterioration [14]. There has been increasing interest in advanced oxidative processes (AOPs) as the most effective approach for the removal of gaseous and liquid pollutants over the last few decades [12–15].

AOPs are becoming more popular as a result of their diverse applications, particularly in the treatment of effluents containing hazardous chemicals and/or refractories [16]. AOPs provide efficient effluent degradation rather than simply altering their phase, as other procedures, such as coagulation/flocculation, filtering, and adsorption, do [17].

In this context, heterogeneous photocatalysis, a new disruptive technique, may be an option for the treatment of these effluents after semiconductor catalysts have led to the total mineralization of organic pollutants to CO_2 and H_2O [13,14,16,17]. Among all semiconductors, titanium dioxide (TiO_2) is one of the most studied semiconductors, owing to its great photochemical stability over a wide pH range, low cost, and lack of toxicity [18]. The synthesis of mixed oxides with doping of different metals, such as metal/TiO_2, as in the case of Zn/TiO_2, is one technique for increasing photocatalyst efficiency. This has demonstrated some favorable properties, such as an increase in support surface area, improved porous structure, and gap energy close to that of TiO_2; however, more research is needed to assess its efficiency, viability, and increase in photocatalytic activity [19–21].

Thus, this work aimed to investigate the effect of Zn doping on TiO_2 supports and different calcination temperatures in the photodiscoloration of aqueous solutions of the reactive dye Orange 122 under solar light.

2. Materials and methods

2.1. Catalysts preparation

The Zn/TiO_2 catalysts were synthesized by the impregnation method, where the metal load of Zn was varied at 2%, 6%, and 10% (m/m), and the calcination temperature was varied between 200°C, 300°C, and 400°C to study the effects of the variables in the process of discoloration of the Orange 122 dye through a 2^2 factorial experiment.

The two levels of the variables, calcination temperature (°C) and Zn (%), are specified in Table 1.

A central point was also included in this experimental design to obtain a second-order response surface model. To calculate the residual error, the central point was repeated three times. As a result, seven experiments were carried out, as shown in Table 2.

2.2. Catalyst synthesis

Zn/TiO_2 (2%, 6% and 10% (m m^{-1}/g g^{-1}) was prepared with TiO_2 (≥91% by Synth) and $ZnCl_2$ (≥97% by Reatec) with ultrapure Milli-Q® water (resistivity of 18 MΩ cm) according to Colpini et al. [14]. The solution was stirred at room temperature in a rotating evaporator for 17 h, evaporated for 1 h at 70°C for solvent removal, and finally dried at 120°C for 21 h. The materials were calcined in a muffle furnace at 200°C, 300°C, and 400°C for 5 h.

2.3. Characterization of catalysts

2.3.1. N_2 adsorption measurements

In a Quantachrome Corporation Model Nova 2000, the specific surface area (S_o), average pore volume (V_p), and average pore diameter (d_p) of the catalysts developed were calculated using N_2 adsorption measurements. By exposing the samples to a previous activation at 150°C in a vacuum for 3 h, the Brunauer–Emmett–Teller (BET) method was used to obtain the S_o values.

2.3.2. Scanning electron microscopy with energy dispersive X-ray spectroscopy

Micrographs of the catalysts were obtained using a Scanning Electron Microscope TESCAN VEGA3, equipped with an energy dispersive X-ray microsound (EDS) Penta FET Precision by OXFORD INSTRUMENTS. The samples were fixed to the surface of double-face adhesive tape and coated with a gold layer.

2.3.3. Point of zero charges

Approximately 1 g of catalyst was weighed, diluted in 30 mL of distilled water, and agitated with a magnetic stirrer

Table 1
Control variables considered in 2^2 factorial design

Variable	Low Level (–1)	Central point (0)	High Level (+1)
Calcination Temp.	200°C	300°C	400°C
% Zn	2	6	10

Table 2
Factorial design data (2^2) with the addition of the central point

Experiment	Zn%	Calcination temperature
1	–1	–1
2	–1	+1
3	+1	–1
4	+1	+1
5	0	0
6	0	0
7	0	0

for 24 h to determine the point of zero charge [12]. After that time, the pH of the suspension was measured with a Luca-Tec pH meter (LUCA-210).

2.3.4. X-ray diffraction

Diffractograms of the catalysts were obtained with a Shimadzu XRD 7000 apparatus. A copper emission line (Cu Kα, λ = 1.54056 Å) with an emission tube acceleration of 30 kV, current of 20 mA, and scanning velocity of 2° 2θ min^{-1} was used as a radiation source.

2.3.5. Photocatalytic tests

2.3.5.1. Dye discoloration under sunlight

The reactive textile dye Orange 122 used in the experiments was obtained from Texpal Química Ltda, located in Valinhos, São Paulo, Brazil. Its chemical structure is presented in Figs. 1 and 2 illustrates the system used.

The experimental equipment included a tank-type reactor in a batch system, a 250 mL beaker, and a magnetic stirrer to ensure that the samples were homogenized throughout the experiment duration (2 h). Each catalyst suspension containing 150 mL of 10 mg L^{-1} aqueous dye solution and 50 mg of catalyst was irradiated with sunlight in the dye discoloration test. Aliquots were taken after reaction times of 0, 30, 60, 90, and 120 min for further discoloration analysis. The aliquots were vacuum filtered using cellulose ester membranes with a diameter of 47 mm and a porosity of 0.22 m. The photocatalysts were tested on March 7 and 8, from 1:30 to 3:30 p.m., when the average solar radiation was measured using a UV radiation meter in the range of 390 to 1,100 nm (Model LI-200, SIMEPAR/Brazil) and ranged from 1,004.6 to 1,314.0 W m^{-2}.

A UV-spectrophotometer, model EEQ-9006 of the Astral Scientifica brand, was used to measure the percentage of discoloration of the solution as a function of time at a wavelength of 486 nm. The calibration curve approach was used to determine the absorbance and the concentrations. Eq. (1) was used to obtain the discoloration percentages.

$$\%\text{Discoloration} = \frac{C_0 - C}{C_0} \times 100 \quad (1)$$

where C_0 is the dye concentration before the test (mg L^{-1}) and C is the dye concentration after the test (mg L^{-1}).

2.3.5.2. Reusability of catalysts

To evaluate catalyst reuse, the tests were performed in the same way as in previous tests (batch reactor; stirrer, 10 mg L^{-1} aqueous solution of dye). However, for evaluation, the photocatalytic activity was evaluated using artificial radiation (mercury vapor lamp 250 W).

2.3.5.3 Discoloration kinetics

To evaluate the discoloration kinetics of the solar photocatalytic process, three models were used: the linearized pseudo-first-order, pseudo-second-order, and Behnajady–Modirshahla–Ghanbery (BMG) models.

Multiple works found in the literature report that pseudo-first-order kinetics are more commonly used regarding the degradation of organic pollutants, especially dyes [22–24]. However, some recent work has reported the use of pseudo-second-order kinetics [19,25] and the BMG model as a good fit for dye discoloration data [26–28]. Thus, in this work, the three kinetic models in Table 3 were used to find the best fit for the Orange 122 dye discoloration data.

2.3.5.4. Statistical analysis

The results of the solar data treatments were obtained using a significance level of the effects of the factors, and

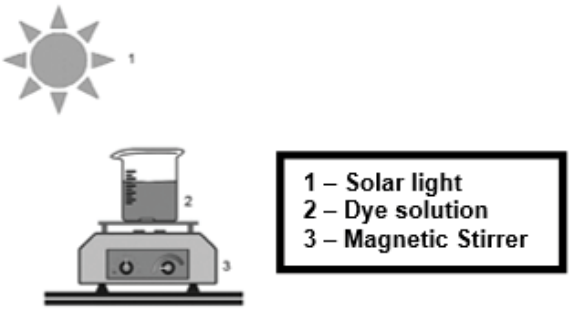

Fig. 2. Schematic diagram of the photocatalytic reactor.

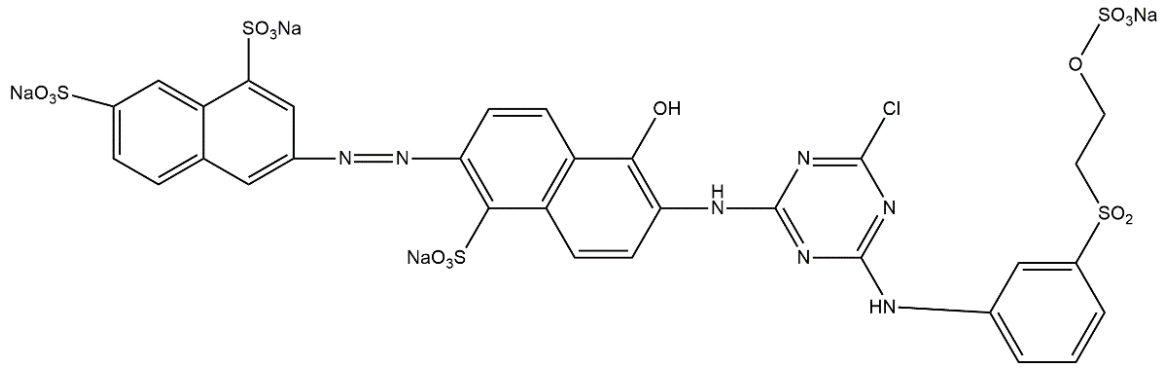

Fig. 1. Chemical structure for Reactive Orange 122 dye.

the interaction was statically tested through analysis of variance (ANOVA) at a level α of the significance of 0.05.

3. Results and discussion

3.1. N_2 adsorption measurements

Fig. 3 shows the N_2 adsorption–desorption isotherms for the materials calcined at 400°C, except for the 6% Zn/TiO_2 catalyst, where the calcination temperature was 300°C.

All the isotherms resembled the Type II isotherm, a typical characteristic of mesoporous materials, based on IUPAC classification [29,30]. Table 4 shows the BET surface areas (S_o), mean pore diameter (d_p), and pore volumes (V_p) of the different catalysts investigated in this study.

The non-calcined TiO_2 catalyst showed a higher surface area of 15.56 $m^2\ g^{-1}$, a pore size of 27.76 Å, and a pore volume of 0.0217 $cm^3\ g^{-1}$ for all catalysts. However, with an increase in the calcination temperature, the surface area decreased, indicating the possibility of slight sintering due to the heat, and another effect of the heat was visible when the pore size of the catalysts increased with the calcination temperature, except for the 10% Zn/TiO_2. Several works in the literature report behavior such as this [13,31,32].

An interesting behavior in the structure of the catalysts was observed when the TiO_2 supports were doped with Zn, and it was expected that an increase in the surface area would occur as more material was added to the support. However, the surface area decreased with increasing metallic load, even at different calcination temperatures. This distinction can be clarified based on the delay in crystallization of the TiO_2 structure due to the presence of Zn

Table 3
Kinetics models used in the experiment

Kinetic model	Equation	References
Pseudo-first-order	$\ln\frac{C_t}{C_o} = k_1 t$	[23]
Pseudo-second-order	$\frac{1}{C_t} - \frac{1}{C_o} = k_2 t$	
BMG	$\frac{t}{1-(C_t/C_o)} = m + bt$	[24]

where C_o and C_t (mg L^{-1}) are the concentrations of the Orange 122 dye at time t = 0 min and time t, respectively, k_1 is the first-order rate constant, k_2 is the second-order rate constant, and m and b are the two constants of BMG model related to the reaction kinetics and oxidative potential.

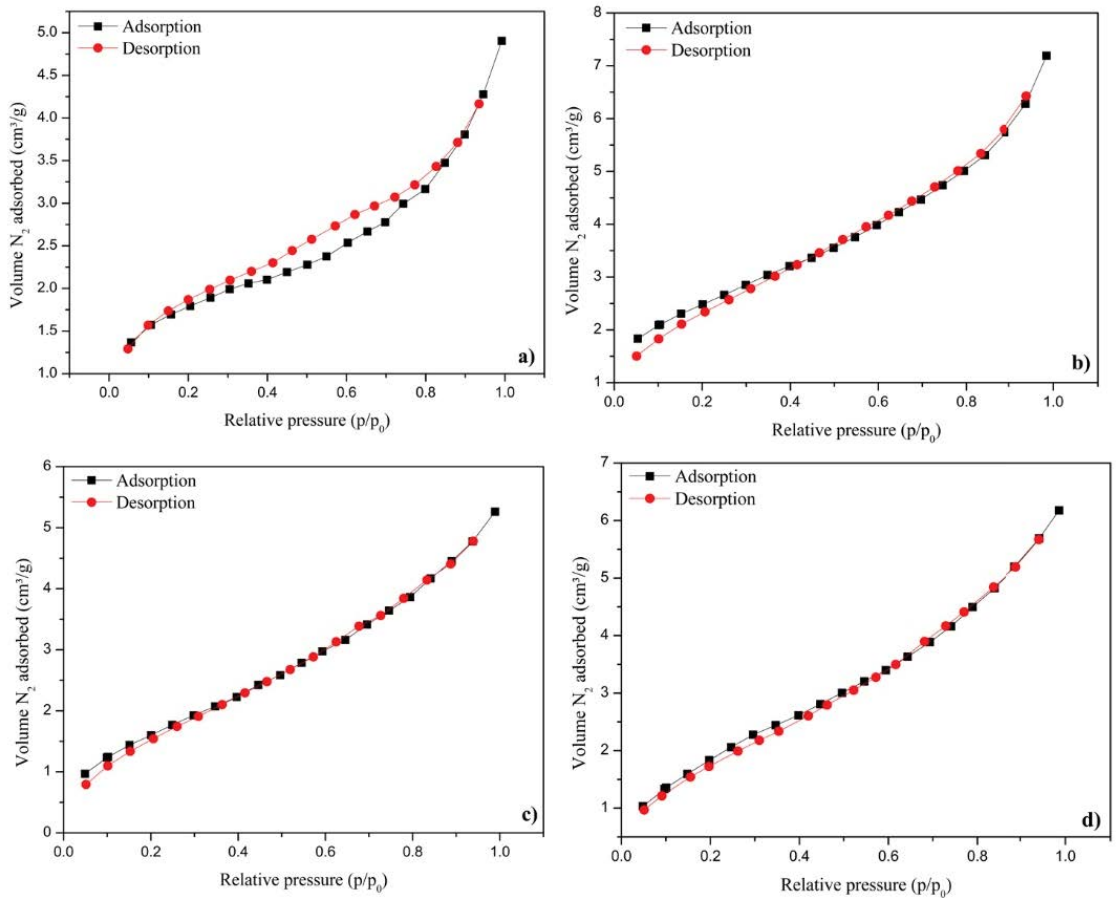

Fig. 3. N_2 adsorption–desorption isotherms for different catalyst samples: (a) TiO_2 – 400°C, (b) 2% Zn/TiO_2 – 400°C, (c) 6% Zn/TiO_2 – 300°C, and (d) 10% Zn/TiO_2 – 400°C.

atoms, which could interfere with the formation of the mesoporous structure itself and may explain the decrease in pore size. As a result, the observed lower surface area for Zn/TiO_2 compared to TiO_2 can be attributed to the lack of a mesoporous structure. Deshmane et al. [30] reported similar behavior for this type of catalyst.

3.2. Scanning electron microscopy with energy dispersive X-ray spectroscopy

Fig. 4 shows the scanning electron microscopy (SEM) micrographs of the co-doped and un-doped TiO_2 catalysts.

Table 4
Textural properties of the catalysts

Catalysts	Calcination temperature	S_o ($m^2\ g^{-1}$)	V_p ($cm^3\ g^{-1}$)	d_p (Å)
TiO_2	Non-calcined	15.56	0.0217	27.76
	200°C	11.12	0.0159	28.56
	300°C	11.36	0.0163	28.61
	400°C	10.98	0.0152	28.76
2% Zn/TiO_2	Non-calcined	6.11	0.0077	24.81
	200°C	9.24	0.0128	27.67
	400°C	8.94	0.0111	24.88
6% Zn/TiO_2	Non-calcined	5.77	0.0074	25.82
	300°C	6.33	0.0081	25.73
10% Zn/TiO_2	Non-calcined	5.76	0.0080	27.74
	200°C	4.92	0.0060	24.62
	400°C	7.71	0.0096	24.80

In all catalysts, a uniform distribution of particles in a spherical shape is observed. Table 5 shows the EDS results for Zn concentration in the catalysts. These results corroborate the proportions proposed during the experiment.

3.3. Point of zero charge

When in solution with a pH higher or lower than its pH_{PZC}, the point of zero charge (PZC), which evaluates the behavior of catalyst surfaces in aqueous solutions, can suggest the tendency of a material's surface to be acidic or basic, indicating that the material is negatively or positively charged [12]. The pH at which the photocatalytic test is performed influences the charge on the catalyst surface and, as a result, the adsorption of contaminants.

The findings of the PZC analysis for the catalysts under investigation are shown in Table 6. The pH_{PZC} of a 10 mg L^{-1} aqueous solution of Reactive Orange 122 dye is approximately 6.0.

Table 6 shows that the catalysts presented different values of pH_{PZC} and consequently different surface charges. For TiO_2 calcined at 200°C, 2% Zn/TiO_2 calcined at 400°C, and 10% Zn/TiO_2 calcined at 400°C, the pH_{PZC} was higher than

Table 5
Analysis of EDS

Catalysts	Zn (wt.%)
2% Zn/TiO_2	2.06
6% Zn/TiO_2	5.24
10% Zn/TiO_2	9.25

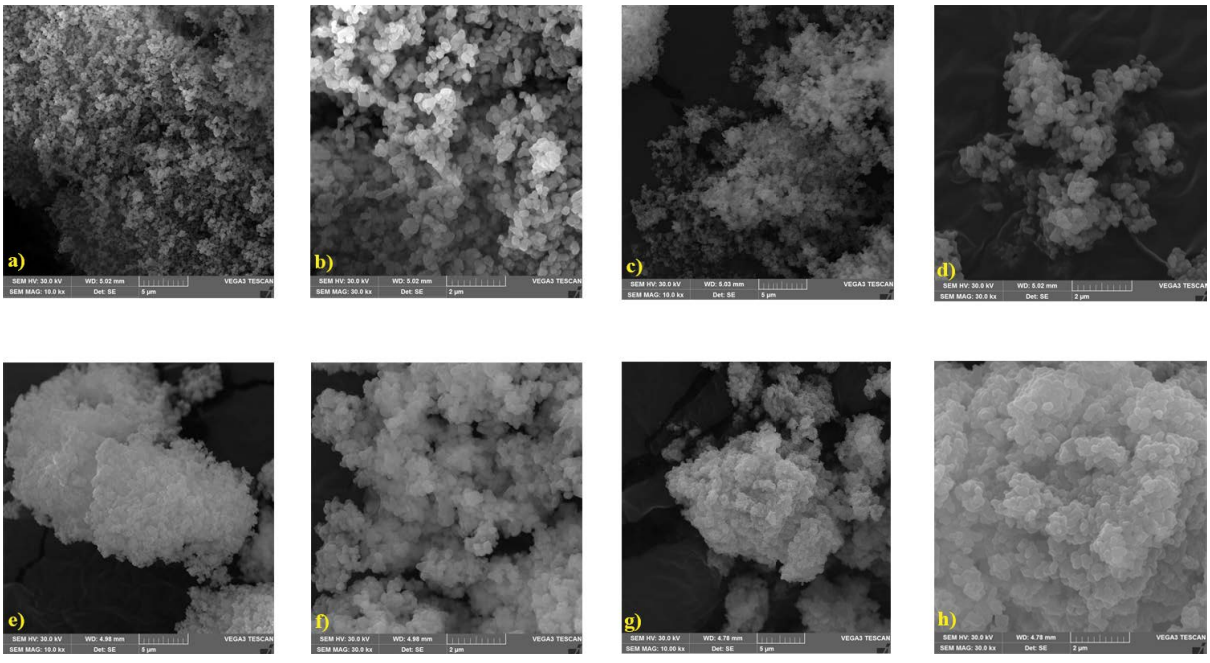

Fig. 4. SEM images of TiO_2 – 400°C in (a) increase: 10.000 x and (b) increase: 30.000 x; 2% Zn/TiO_2 – 400°C in (c) increase: 10.000 x and (d) increase: 30.000 x; 6% Zn/TiO_2 – 300°C in (e) increase: 10.000 x and (f) increase: 30.000 x; 10% Zn/TiO_2 – 400°C in (g) increase: 10.000 x and (h) increase: 30.000 x.

the pH of the solution, which indicates that the surface is negatively charged. The other catalysts presented a pH_{PZC} lower than the pH of the solution, which indicates that the surface is positively charged.

3.4. X-ray diffraction

X-ray diffraction (XRD) patterns of the TiO_2 and Zn/TiO_2 catalysts are shown in Fig. 5.

In Fig. 5a all present peaks at 27°, 36°, 39°, 41°, 44°, 54°, 56°, 64°, and 69° are related to the rutile phase (tetragonal) of TiO_2, according to JCPDS card n° 87–0710 [33], not showing other crystalline phases, such as anatase and brookite [21,34]. It was also possible to observe that no zinc-related peak was found, and with the detection limit of XRD, these samples appear as a single-phase rutile, even though the SEM/EDS analysis shows otherwise, and this behavior was reported in other works of the literature [35,36].

In addition, it is known that the ionic radius of Zn^{2+} ions is higher than that of Ti^{4+} ions (Zn^{2+}: 74 pm, Ti^{4+}: 68 pm) [35,37]. An increase in lattice parameters and cell volume is expected if the Zn^{2+} ions replace the Ti^{4+} ions in the lattice. In Fig. 5b it is possible to observe that the lines shrank to smaller values with the increase in the metallic charge of Zn (6% and 10%) in the catalyst; earlier literature reports similar behavior [36,38]. This shift corresponds to a contraction of the c-axis of the rutile lattice thanks to the presence of the Zn^{2+} dopant of the TiO_2 lattice, which confirms the presence of Zn in the TiO_2 rutile structure. Another explanation for the non-appearance of the peaks would be that the Zn ions are not doped in the interstices of the TiO_2 crystal lattice, possibly because they are highly dispersed in the material [12].

In Table 7, the lattice parameters and cell volume are shown, indicating a decrease in the value of c, which corroborates the observations in Fig. 5b.

Table 6
PZC results

Catalysts	Calcination temperature (°C)	pH_{PZC}
TiO_2	200	7.40
	300	5.87
	400	4.65
2% Zn/TiO_2	200	295
	400	6.48
6% Zn/TiO_2	300	5.77
10% Zn/TiO_2	200	5.56
	400	6.12

3.5. Photocatalytic tests

3.5.1. Dye discoloration under sunlight

Fig. 6 presents the photocatalytic discoloration of an aqueous solution of the reactive dye Orange 122 in 2 h under solar radiation.

In Fig. 6, it is possible to observe that the doping of Zn in the TiO_2 supports had a significant influence on the discoloration of the solution of the reactive dye Orange 122, not necessarily on the amount of doped metal; catalysts with 2% and 6% Zn reached a discoloration of approximately 100%, as seen in Fig. 6a and b.

Another factor that influenced the discoloration of the solution of the reactive dye Orange 122 was the temperature. Fig. 6 shows that a low calcination temperature resulted in a higher discoloration rate. These results corroborate those in Table 4, where catalysts calcined at a low temperature generally presented a higher surface area, contributing to a higher percentage of discoloration.

In addition, the different surface charges had a significant effect on the dye discoloration process, and the catalysts that presented a positive surface charge had the highest discoloration values. This can be explained by the interaction between the negative charges present in the dye solution and the positive surface charge of the catalyst, which favors the discoloration process since an adsorptive process occurs through electrostatic interaction between the two species, which does not occur among catalysts with negative

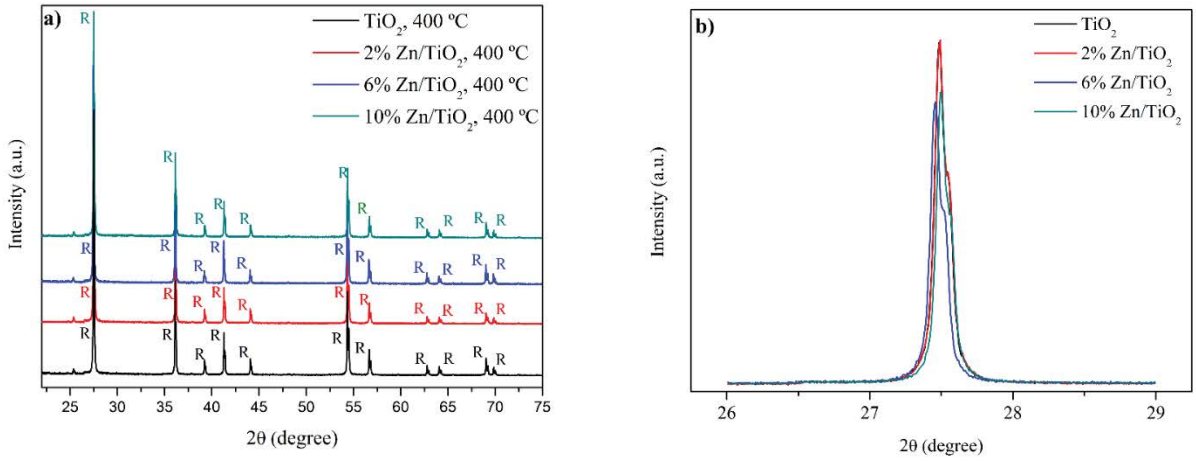

Fig. 5. X-ray diffraction patterns for the catalysts: (a) full 2θ run (R: rutile) and (b) expansion of 2θ for plan (101).

Table 7
Lattice parameters and cell volume

Catalysts	Calcination temperature (°C)	Lattice parameters (Å)			Cell volume (Å)
		A	*B*	*C*	
TiO_2	400	4.593	4.593	2.958	62.415
2% Zn/TiO_2		4.593	4.593	2.958	62.415
6% Zn/TiO_2		4.593	4.593	2.834	59.785
10% Zn/TiO_2		4.593	4.593	2.852	60.165

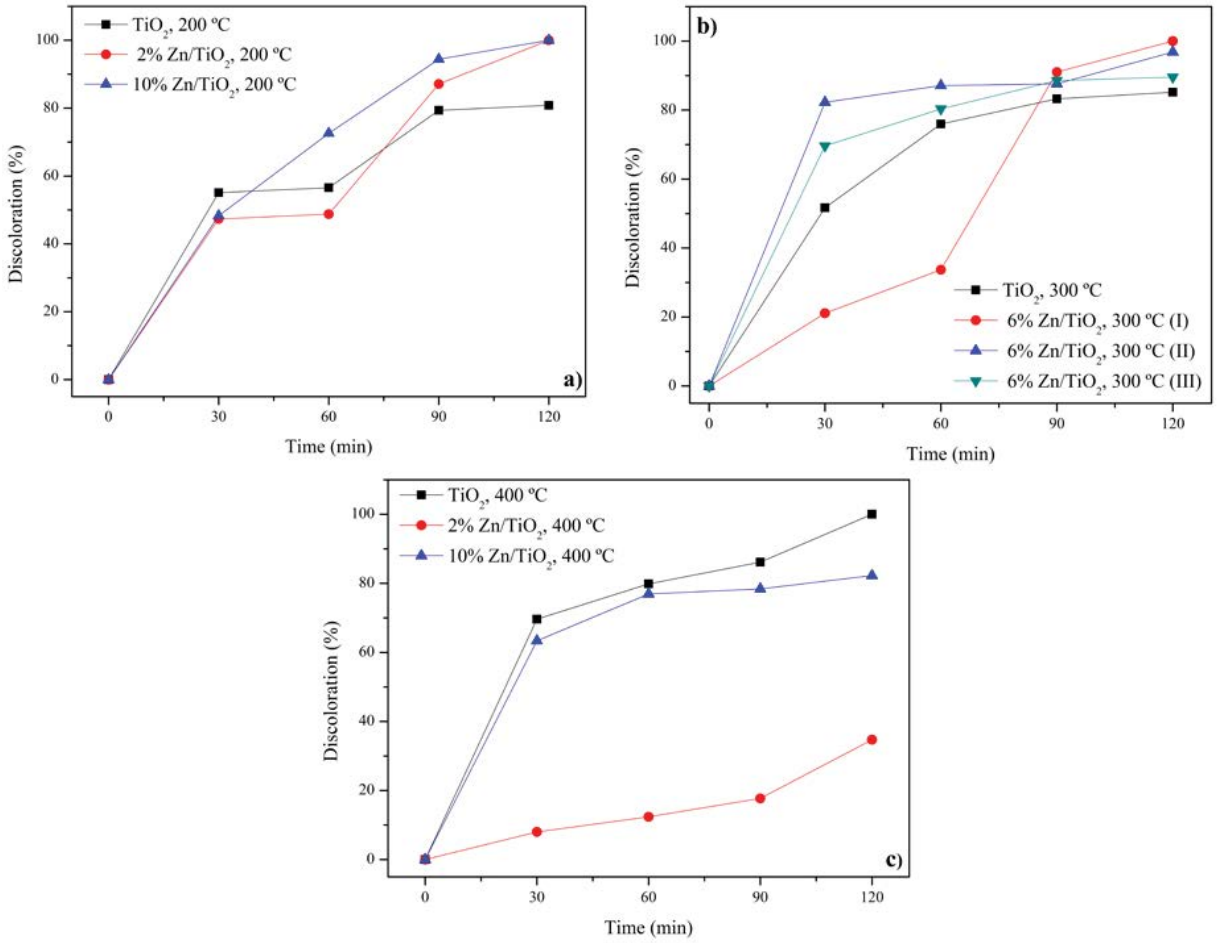

Fig. 6. Photocatalytic discoloration of the aqueous solution of reactive dye Orange 122 dye with catalysts: (a) calcined at 200°C, (b) calcined at 300°C, and (c) calcined at 400°C.

surface charge, such as TiO_2 calcined at 200°C, 2% Zn/TiO_2 calcined at 400°C, and 10% Zn/TiO_2 calcined at 400°C, since an electrostatic repulsion phenomenon occurs between the surface of the catalysts and the dye molecules, making the adsorption process difficult and the photocatalytic process governing during the discoloration of the solutions [39,40].

In Fig. 7, it is possible to observe how the discoloration process occurred over time for the catalyst 2% Zn/TiO_2 calcined at 200°C.

3.5.2. Reusability of catalysts

Fig. 8 shows the reusability of the studied catalysts for the photodiscoloration of Orange 122 over four cycles under UV irradiation.

The Orange 122 dye concentration was adjusted each time to its initial value. The catalysts were reused for four cycles. It was observed that the smaller the amount of Zn in the catalyst was, the lower the stability. All catalysts had a significant decline from the first to the last cycle.

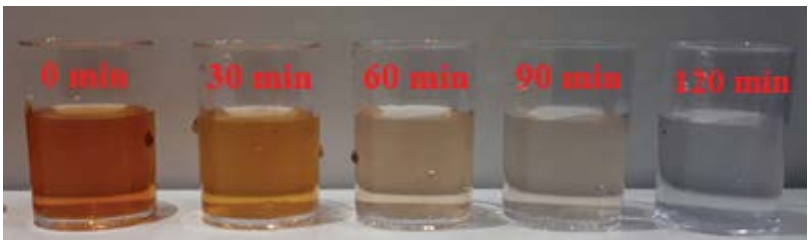

Fig. 7. Illustration of the discoloration process for the catalysts 2% Zn/TiO_2 calcined at 200°C.

The discoloration in the first reuse cycle for the TiO_2, 2% Zn/TiO_2, 6% Zn/TiO_2 and 10% Zn/TiO_2 catalysts was 76%, 97%, 100% and 95%, respectively. In the last cycle, TiO_2, 2% Zn/TiO_2, 6% Zn/TiO_2, and 10% Zn/TiO_2 obtained 20%, 30%, 33% and 32%, respectively, in the photodiscoloration of Orange 122.

Teixeira et al. [41] studied the use of TiO_2 and ZnO (5%, 10%, and 15%) immobilized in poly-(vinylidene difluoride)-co-trifluoroethylene on the photocatalytic degradation of methylene blue. The authors verified that after the third use of the catalyst, there was a loss in the photocatalytic activity; they related this phenomenon to the possible presence of organic contaminants on the semiconductor surface from the second use, which thus competed for the active sites available on the photocatalyst.

However, Chen et al. [42], when using ZnO catalysts synthesized by the sol-gel method in the degradation of azo dyes (Methyl orange, Congo red, and Direct black), found that after 4 cycles, the catalyst showed an average reduction in the catalytic activity of 6%, probably due to the inevitable loss of photocatalysts during the reuse processes, according to the authors.

Madan et al. [43] applied nanoflock-shaped ZnO catalysts on the surface of a zeolite for Congo red dye photodegradation and adsorption. As in the aforementioned research, the authors also found a loss of photocatalytic activity of the material, a value close to 17% after 5 cycles.

3.5.3. Discoloration kinetics

The kinetic parameters for the discoloration assays were obtained by applying a linear regression analysis on the three models, $\ln(C_o/C_t)$ vs. t data for the pseudo-first-order model, $[(1/C_t)–(1/C_o)]$ vs. t data for the pseudo-second-order model and $t/[1–(C_t/C_0)]$ vs. t data for the BMG model. Table 8 shows the obtained kinetic parameters.

It was possible to observe that the fitting of pseudo-first-order and pseudo-second-order kinetic experimental data were not good, as the correlation coefficients were the lowest. However, the values of the correlation coefficients for the BMG model are higher than those for the pseudo-first-order and pseudo-second-order models, indicating that the BMG model was the one that best fit the data. Other reports in the literature using AOP stated that the BMG model presented the best fit for the discoloration data of textile dyes such as Yellow 17, Methyl Orange, Acid Yellow 23, Acid Red 66, and Direct Blue 71 [26–28,44].

3.5.4. Statistical analysis

Fig. 9 shows a geometrical representation of the complete factorial design (2^2) with the central point addition. The horizontal axis represents the variable Zn, while the vertical axis represents the variable calcination temperature. Each vertex of the picture represents the result of the experiment. The average of the findings obtained with the central point is 95.03 in the center of the image.

Through the statistical analysis, it was possible to understand how the factors interact with the response variable in an isolated way and between them. Fig. 10 shows the Pareto chart.

From the Pareto chart, it was possible to observe that Factor B – calcination temperature – had a significant statistical effect on the response variable and can be verified by ANOVA.

Table 8
Kinetic parameters of the models and their adjusted determination coefficient (Adj. R^2)

Catalysts	Calcination temperature (°C)	k_1	Adj. R^2	k_2	Adj. R^2	m	b	Adj. R^2
TiO_2	200	0.0153	0.9440	0.0036	0.9564	29.3417	1.0107	0.9826
	300	0.0184	0.9519	0.0050	0.9898	28.4101	0.9036	0.9976
	400	0.0422	0.8558	0.0076	0.9872	17.3886	0.9117	0.9947
2% Zn/TiO_2	200	0.0397	0.8245	0.0070	0.9006	70.5442	0.4232	0.9723
	400	0.0003	0.9395	0.0003	0.9138	709.5970	–2.9680	0.9860
6% Zn/TiO_2	300	0.0399	0.8265	0.0080	0.8517	142.1380	–0.2366	0.9686
	300	0.0288	0.9048	0.0180	0.8263	6.1528	1.0265	0.9974
10% Zn/TiO_2	300	0.0222	0.9137	0.0076	0.9869	13.3273	1.0001	0.9996
	200	0.0439	0.8955	0.0108	0.7828	43.5168	0.6190	0.9984
	400	0.0172	0.8489	0.0042	0.9590	13.8761	1.1005	0.9994

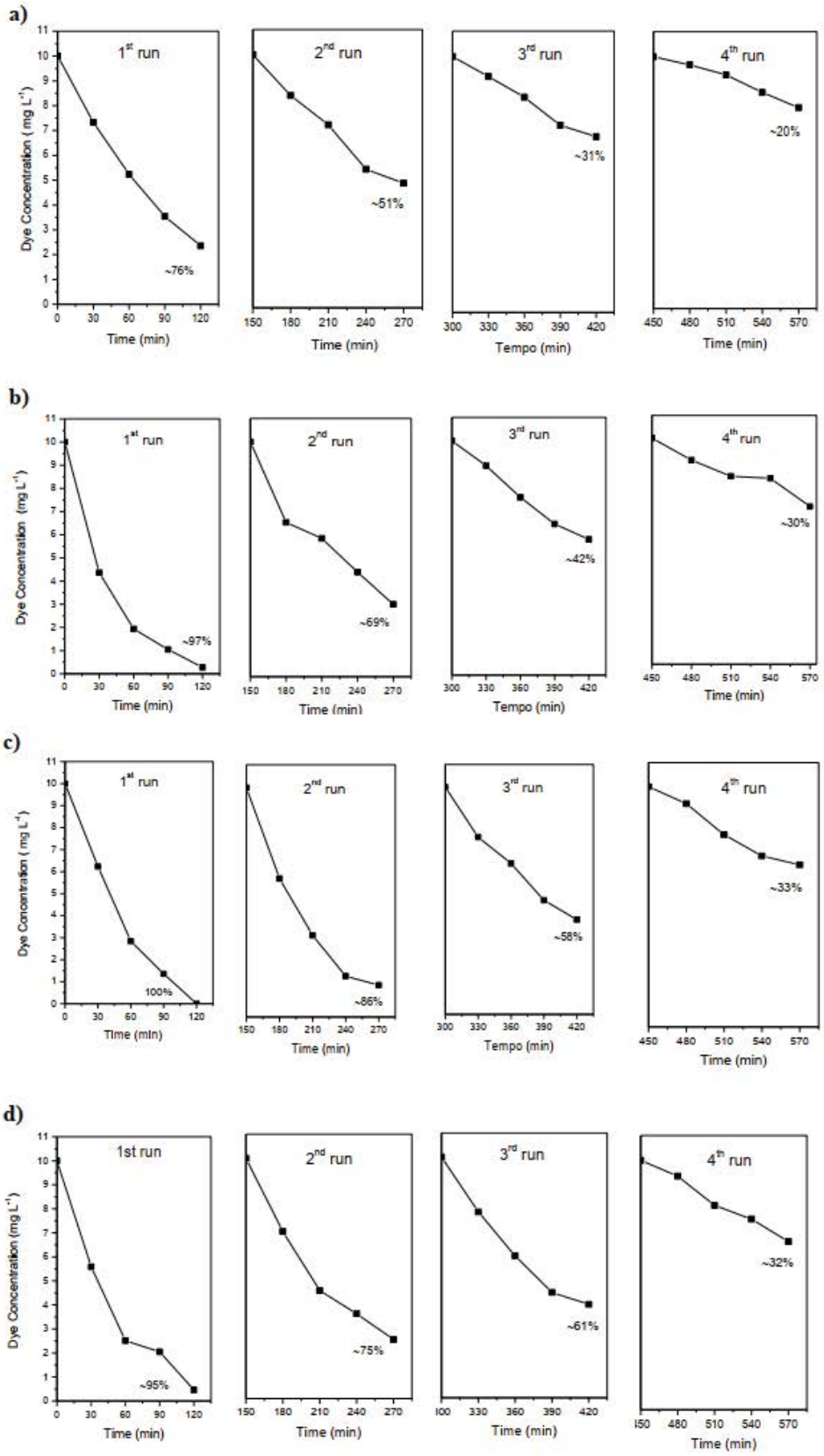

Fig. 8. Effect of reusability (a) TiO_2, calcined at 400°C, (b) 2% Zn/TiO_2, calcined at 200°C, (c) 6% Zn/TiO_2, calcined at 300°C, and (d) 10% Zn/TiO_2 calcined at 200°C.

Through ANOVA, it was also possible to observe that the calcination temperature had a significant effect on the discoloration of the dye, with a p-value < 0.05 was obtained, and the residual error was $\sqrt{23.33} = 4.83$, as shown in Table 9.

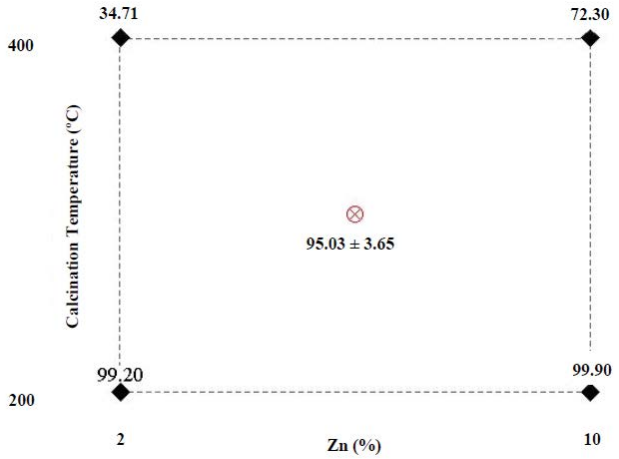

Fig. 9. Geometric vision of 2^2 design.

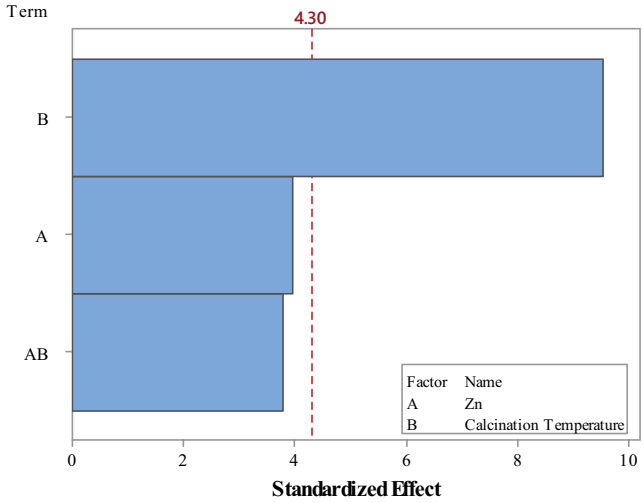

Fig. 10. Pareto chart of the standardized effect, for α = 0.05.

The results of the effect of the main factors, Zn and calcination temperature, are given in Table 9 and shown in Fig. 11.

In Fig. 11a, it is possible to note that Zn content has practically no significant effect on dye discoloration, as the mean percentage of discoloration at the lower concentration level (2%) is close to the higher concentration level (10%).

However, in Fig. 11b it is observed that the effect of the calcination temperature was strongly significant, since the average percentage of discoloration at the lower temperature level presented a value of 100%, which was higher than the percentage of discoloration at the higher temperature level, which was close to 53%.

Since the main goal is to maximize the percentage of dye discoloration, Fig. 11 indicates that it would be best to adjust the calcination temperature to a lower level, as the descending slope of the line indicates that the lower the temperature is, the higher the percentage of discoloration [45,46].

Fig. 12 shows the interaction plot between the two variables in the study.

It is also noted, both through the ANOVA test (Table 9) and Fig. 12, that the interaction between the Zn content and the calcination temperature had a weak statistical effect on the process of dye discoloration. In addition, the Zn content does not have a major influence on the discoloration, as shown in Fig. 12.

It becomes clear if we look at Fig. 12 that the best fit would be to fix the temperature at the lower level (200°C) when for both Zn levels the percentage of dye discoloration was approximately 100%.

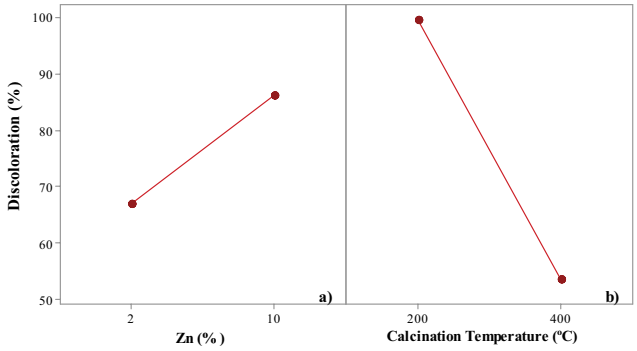

Fig. 11. Effect of the main factors analyzed: (a) Zn (%) and (b) calcination temperature (°C).

Table 9
ANOVA results for the quadratic model of the response surface

Source	DF	Discoloration			
		Sum of squares	Mean square	F-value	p-value
Temperature	1	2,124.29	2,124.29	91.04	0.0108
Zn	1	368.26	368.26	25.10	0.0576
Temperature^2	1	585.66	585.66	25.10	0.0579
Zn × Temperature	1	338.56	338.56	14.51	0.0625
Residual	2	46.67	23.33		
Total	6	3,463.43	577.24		
		$R^2 = 0.9865$	$R^2_{adj} = 0.9596$		

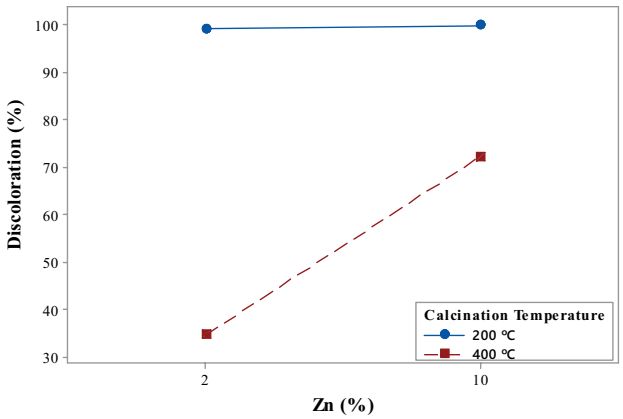

Fig. 12. Zn vs. calcination temperature interaction.

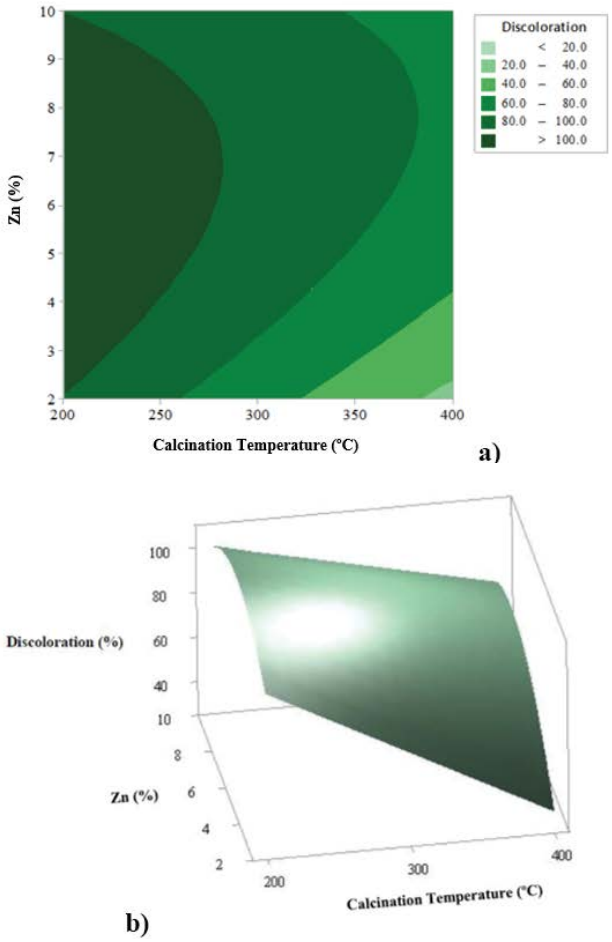

Fig. 13. Second-order response surface model plot: (a) level curves and (b) response surface.

Finally, a second-order response surface model was obtained by using ordinary least squares. The regression model with an adjusted regression coefficient (R^2_{adj} = 0.960) is represented by Eq. (2):

$$y = 149.6 + 9.36x_1 - 0.3685x_2 - 1.155x_1^2 + 0.023x_1x_2 \quad (2)$$

where x_1 is the Zn content (%), x_2 is the calcination temperature (°C) and y is the percentage of dye discoloration.

Fig. 13 shows the second-order response surface model plot obtained.

From Fig. 13, it was possible to observe that the optimal fit that maximizes the percentage of dye discoloration is obtained by fixing the calcination temperature at 200°C, which would give an expected percentage of discoloration of approximately 100%.

4. Conclusions

In this work, Zn/TiO_2 catalysts were successfully obtained by the impregnation method, and the variation in the factors Zn and calcination temperature had a significant effect on the percentage of discoloration of an aqueous solution of the reactive dye Orange 122.

From the statistical analysis, it was possible to conclude that Zn load does not have a significant effect on the percentage of discoloration. The calcination temperature had a major effect, with the best fit being to fix the value at 200°C, where a percentage of discoloration of approximately 100% was obtained.

These results allow the production of new studies investigating different ranges of calcination temperatures and metallic loads of Zn. In addition to finding the best optimization values, one process at higher temperatures and high quantities of metal increases the value of the synthesis of these materials.

Declaration of competing interest

The authors declare that they have no known competing financial interests or personal relationships that could have appeared to influence the work reported in this paper.

References

[1] C.P. Sajan, B. Shahmoradi, H.P. Shivaraju, K.M. Lokanatha Rai, S. Ananda, M.B. Shayan, T. Thonthai, G.V. Narasimha Rao, K. Byrappa, Photocatalytic degradation of textile effluent using hydrothermally synthesized titania supported molybdenum oxide photocatalyst, Mater. Res. Innovations, 14 (2010) 89–94.

[2] K. Salehi, B. Shahmoradi, A. Bahmani, M. Pirsaheb, H.P. Shivaraju, Optimization of reactive black 5 degradations using hydrothermally synthesized NiO/TiO_2 nanocomposite under natural sunlight irradiation, Desal. Water Treat., 57 (2016) 25256–25266.

[3] B. Shahmoradi, M.A. Pordel, M. Pirsaheb, A. Maleki, S. Kohzadi, Y. Gong, R.R. Pawar, S.-M. Lee, H.P. Shivaraju, G. McKay, Synthesis and characterization of barium-doped TiO_2 nanocrystals for photocatalytic degradation of Acid red 18 under solar irradiation, Desal. Water Treat., 88 (2017) 200–206.

[4] M.S. Sadjadi, M. Mozaffari, M. Enhessari, K. Zare, Effects of $NiTiO_3$ nanoparticles supported by mesoporous MCM-41 on photoreduction of methylene blue under UV and visible light irradiation, Superlattices Microstruct., 47 (2010) 685–694.

[5] H. Kusic, N. Koprivanac, A.L. Bozic, Environmental aspects on the photodegradation of reactive triazine dyes in aqueous media, J. Photochem. Photobiol., A, 252 (2013) 131–144.

[6] T.R. Giraldi, J.P. Swerts, M.A. Vicente, V.R. de Mendonça, E.C. Paris, C. Ribeiro, Use of ZnO:Mn particles for the degradation of methylene blue by photocatalysis process, Cerâmica, 62 (2016) 345–350.

[7] S. Lalnunhlimi, V. Krishnaswamy, Decolorization of azo dyes (Direct Blue 151 and Direct Red 31) by a moderately alkaliphilic bacterial consortium, Braz. J. Microbiol., 47 (2016) 39–46.
[8] C.S.D. Rodrigues, S.A.C. Carabineiro, F.J. Maldonado-Hódar, L.M. Madeira, Wet peroxide oxidation of dye-containing wastewaters using nanosized Au supported on Al_2O_3, Catal. Today, 280 (2017) 165–175.
[9] M. Qamar, M. Saquib, M. Muneer, Photocatalytic degradation of two selected dye derivatives, chromotrope 2B and amido black 10B, in aqueous suspensions of titanium dioxide, Dyes Pigm., 65 (2005) 1–9.
[10] S.B. Khan, M. Hou, S. Shuang, Z. Zhang, Morphological influence of TiO_2 nanostructures (nanozigzag, nanohelics and nanorod) on photocatalytic degradation of organic dyes, Appl. Surf. Sci., 400 (2017) 184–193.
[11] M. Pirsaheb, B. Shahmoradi, T. Khosravi, K. Karimi, Y. Zandsalimi, Solar degradation of malachite green using nickel-doped TiO_2 nanocatalysts, Desal. Water Treat., 57 (2015) 9881–9888.
[12] L.E.N. de Castro, E.C. Meurer, H.J. Alves, M.A.R. dos Santos, E. de C. Vasques, L.M.S. Colpini, Photocatalytic degradation of textile dye Orange 122 via electrospray mass spectrometry, Braz. Arch. Biol. Technol., 63 (2020), doi: 10.1590/1678-4324-2020180573.
[13] L.M.S. Colpini, G.G. Lenzi, M.B. Urio, D.M. Kochepka, H.J. Alves, Photodiscoloration of textile reactive dyes on Ni/TiO_2 prepared by the impregnation method: effect of calcination temperature, J. Environ. Chem. Eng., 2 (2014) 2365–2371.
[14] L.M.S. Colpini, H.J. Alves, O.A.A. dos Santos, C.M.M. Costa, Discoloration and degradation of textile dye aqueous solutions with titanium oxide catalysts obtained by the sol–gel method, Dyes Pigm., 76 (2008) 525–529.
[15] J.C. Medina, M. Bizarro, P. Silva-Bermudez, M. Giorcelli, A. Tagliaferro, S.E. Rodil, Photocatalytic discoloration of methyl orange dye by δ-Bi2O_3 thin films, Thin Solid Films, 612 (2016) 72–81.
[16] M.C.P. Souza, G.G. Lenzi, L.M.S. Colpini, L.M.M. Jorge, O.A.A. Santos, Photocatalytic discoloration of reactive blue 5G dye in the presence of mixed oxides and with the addition of iron and silver, Braz. J. Chem. Eng., 28 (2011) 393–402.
[17] R.L. Narayana, M. Matheswaran, A.A. Aziz, P. Saravanan, Photocatalytic decolourization of basic green dye by pure and Fe, Co doped TiO_2 under daylight illumination, Desalination, 269 (2011) 249–253.
[18] B. Shahmoradi, I.A. Ibrahim, N. Sakamoto, S. Ananda, T.N. Guru Row, K. Soga, K. Byrappa, S. Parsons, Y. Shimizu, *In situ* surface modification of molybdenum-doped organic–inorganic hybrid TiO_2 nanoparticles under hydrothermal conditions and treatment of pharmaceutical effluent, Environ. Technol., 31 (2010) 1213–1220.
[19] K.-S. Lin, Y.-G. Lin, H.-W. Cheng, Y.-H. Haung, Preparation and characterization of V-Loaded titania nanotubes for adsorption/photocatalysis of basic dye and environmental hormone contaminated wastewaters, Catal. Today, 307 (2018) 119–130.
[20] H. Meng, B. Wang, S. Liu, R. Jiang, H. Long, Hydrothermal preparation, characterization and photocatalytic activity of TiO_2/Fe–TiO_2 composite catalysts, Ceram. Int., 39 (2013) 5785–5793.
[21] J. Deng, M. Wang, J. Fang, X. Song, Z. Yang, Z. Yuan, Synthesis of Zn-doped TiO_2 nano-particles using metal Ti and Zn as raw materials and application in quantum dot sensitized solar cells, J. Alloys Compd., 791 (2019) 371–379.
[22] T. Dong, J. Tong, C. Bian, J. Sun, S. Xia, Experimental study and kinetic analysis of oxidant-free thermal-assisted UV digestion utilizing supported nano-TiO_2 photocatalyst for detection of total phosphorous, Chin. J. Chem. Eng., 23 (2015) 93–99.
[23] H. Khan, N. Ahmad, A. Yasar, R. Shahid, Advanced oxidative decolorization of Red Cl5B, Pol. J. Environ. Stud., 19 (2010) 83–92.
[24] J. da S. Lopes, W.V. Rodrigues, V.V. Oliveira, A. do N.S. Braga, R.T. da Silva, A.A.C. França, E.C. da Paz, J.A. Osajima, E.C. da Silva Filho, Modification of kaolinite from Pará/Brazil region applied in the anionic dye photocatalytic discoloration, Appl. Clay Sci., 168 (2019) 295–303.
[25] M. Kheirabadi, M. Samadi, E. Asadian, Y. Zhou, C. Dong, J. Zhang, A.Z. Moshfegh, Well-designed Ag/ZnO/3D graphene structure for dye removal: adsorption, photocatalysis and physical separation capabilities, J. Colloid Interface Sci., 537 (2019) 66–78.
[26] N. Bougdour, A. Sennaoui, I. Bakas, A. Assabbane, Experimental evaluation of Reactive Yellow 17 degradation using UV light and iron ions activated peroxydisulfate: efficiency and kinetic model, Sci. Technol. Mater., 30 (2018) 157–165.
[27] H.-Y. Xu, T.-N. Shi, L.-C. Wu, S.-Y. Qi, Discoloration of Methyl orange in the presence of schorl and H_2O_2: kinetics and mechanism, Water Air Soil Pollut., 224 (2013), doi: 10.1007/s11270-013-1740-9.
[28] S. Tunç, T. Gürkan, O. Duman, On-line spectrophotometric method for the determination of optimum operation parameters on the decolorization of Acid Red 66 and Direct Blue 71 from aqueous solution by Fenton process, Chem. Eng. J., 181–182 (2012) 431–442.
[29] K.S.W. Sing, Reporting physisorption data for gas/solid systems with special reference to the determination of surface area and porosity, Pure Appl. Chem., 57 (1985) 603–619.
[30] V.G. Deshmane, S.L. Owen, R.Y. Abrokwah, D. Kuila, Mesoporous nanocrystalline TiO_2 supported metal (Cu, Co, Ni, Pd, Zn, and Sn) catalysts: effect of metal-support interactions on steam reforming of methanol, J. Mol. Catal. A: Chem., 408 (2015) 202–213.
[31] L.M.S. Colpini, G.G. Lenzi, R.C.T. de Souza, M.B. Urio, D.M. Kochepka, M.A.R. Santos, E.C. Vasques, H.J. Alves, Photodiscoloration processes of dyes reactive using radiation and Fe/TiO_2, Int. J. Mater. Eng. Technol., 15 (2017) 189–204.
[32] G.G. Lenzi, R.F. Evangelista, E.R. Duarte, L.M.S. Colpini, A.C. Fornari, R. Menechini Neto, L.M.M. Jorge, O.A.A. Santos, Photocatalytic degradation of textile reactive dye using artificial neural network modeling approach, Desal. Water Treat., 57 (2015) 14132–14144.
[33] JCPDS, International Centre for Diffraction Data, PCPDFWIN, 1997.
[34] M.S. Lassoued, A. Lassoued, M.S.M. Abdelbaky, S. Ammar, A. Gadri, A. Ben Salah, S. García-Granda, Influence of iron doping on the photocatalytic activity of nanocrystalline TiO_2 particles fabricated by ultrasound method for enhanced degradation of organic dye, J. Mater. Sci. Mater. Electron., 29 (2018) 6019–6031.
[35] S. Yan, Y. Yu, Y. Gu, Y. Liu, Y. Cao, Improved photocatalytic activity of TiO_2 modified with unique O–Zn–Cl surface species, Sep. Purif. Technol., 171 (2016) 118–122.
[36] R.G. Nair, S. Mazumdar, B. Modak, R. Bapat, P. Ayyub, K. Bhattacharyya, The role of surface O-vacancies in the photocatalytic oxidation of Methylene Blue by Zn-doped TiO_2: a mechanistic approach, J. Photochem. Photobiol., A, 345 (2017) 36–53.
[37] K.-P. Wang, H. Teng, Zinc-doping in TiO_2 films to enhance electron transport in dye-sensitized solar cells under low-intensity illumination, Phys. Chem. Chem. Phys., 11 (2009) 9489–9496.
[38] Y.-H. Zhang, C.K. Chan, J.F. Porter, W. Guo, Micro-Raman spectroscopic characterization of nanosized TiO_2 powders prepared by vapor hydrolysis, J. Mater. Res., 13 (1998) 2602–2609.
[39] L.E.N. Castro, F. Meurer, L.M.S. Colpini, Study of the application of brewers' spent grains as an adsorbent for the removal of lubricating oil in an aqueous medium, Braz. J. Dev., 7 (2021) 120522–120527.
[40] L.E.N. Castro, J.V.F. Santos, K.C. Fagnani, H.J. Alves, L.M.S. Colpini, Evaluation of the effect of different treatment methods on sugarcane vinasse remediation, J. Environ. Sci. Health., Part B, 54 (2019) 791–800.
[41] S. Teixeira, P.M. Martins, S. Lanceros-Méndez, K. Kühn, G. Cuniberti, Reusability of photocatalytic TiO_2 and ZnO nanoparticles immobilized in poly(vinylidene difluoride)-co-trifluoroethylene, Appl. Surf. Sci., 384 (2016) 497–504.

[42] X. Chen, Z. Wu, D. Liu, Z. Gao, Preparation of ZnO photocatalyst for the efficient and rapid photocatalytic degradation of azo dyes, Nanoscale Res. Lett., 12 (2017), doi: 10.1186/s11671-017-1904-4.
[43] S. Madan, R. Shaw, S. Tiwari, S.K. Tiwari, Adsorption dynamics of Congo red dye removal using ZnO functionalized high silica zeolitic particles, Appl. Surf. Sci., 487 (2019) 907–917.
[44] M.A. Behnajady, N. Modirshahla, F. Ghanbary, A kinetic model for the decolorization of C.I. Acid Yellow 23 by Fenton process, J. Hazard. Mater., 148 (2007) 98–102.
[45] W.G. Sganzerla, A.P.G. da Silva, L.E.N. Castro, C.G. da Rosa, R.A. Komatsu, M.R. Nunes, J.P. Ferrareze, A.P. de L. Veeck, Chemometric approach based on multivariate analysis for discriminating uvaia (*Eugenia pyriformis*) fruits during the ripening stages: physicochemical characteristics, bioactive compounds, and antioxidant activity, JSFA Rep., 2 (2022) 178–186.
[46] L.E.N. Castro, L.M.S. Colpini, Effect of temperature on the moisture adsorption process in brewers' spent grains, Braz. J. Dev., 8 (2022) 30389–30399.